Photoinduced electron transfer from enol silyl ethers to quinone. Part 2.[1] Direct observation of ion-pair dynamics by time-resolved spectroscopy

T. Michael Bockman and Jay K. Kochi*

Department of Chemistry, University of Houston, Houston, TX 77204-5641, USA

Time-resolved spectroscopy in two time domains (encompassing picoseconds and nanoseconds/microseconds) allows all the reactive intermediates involved in the photooxidation of enol silyl ethers (ESE) by chloranil (CA) to be identified, and each step in their temporal evolution to α-enone (E) and adduct (A) to be delineated. Thus, the radical-ion pair [ESE$^{\bullet+}$, CA$^{\bullet-}$] is the common intermediate formed in unit quantum yield *via* the highly efficient quenching of triplet chloranil by enol silyl ethers in both dichloromethane and acetonitrile. In the context of the Fuoss–Winstein formulation, the first-formed [ESE$^{\bullet+}$, CA$^{\bullet-}$] is a contact ion-pair, which in a non-polar solvent, such as dichloromethane, predominantly suffers an initial ion-pair collapse (internal return) by β-proton transfer, and the resultant radical pair ultimately leads to α-enone (E). The contact ion-pair formed in the polar solvent undergoes diffusive separation, and the free ion ESE$^{\bullet+}$ suffers desilylation by acetonitrile and ultimately leads to adduct (A). Added electrolyte to dichloromethane solutions modulates the ion-pair behaviour *via* the 'special salt effect' to divert the enone pathway to adduct formation.

Introduction

Product studies stemming from solvent and salt effects on the photooxidation of enol silyl ethers (ESE) with chloranil (CA) (tetrachloro-1,4-benzoquinone), as described in the foregoing study,[1] indicate that the radical-ion pair [ESE$^{\bullet+}$, CA$^{\bullet-}$] is formed as the common intermediate in the pathway to produce the ultimate products, α-enone (**E**) and adduct (**A**). Indeed, the competitive formation of these two products, as modulated by solvent polarity and added salt, provides a unique opportunity to establish the complete ion-pair dynamics in a prototypical photoinduced electron-transfer process. Accordingly, we now show how the recent developments in time-resolved spectroscopy[2] allow the temporal events leading to electron-transfer quenching and the formation of the radical-ion pair [ESE$^{\bullet+}$, CA$^{\bullet-}$] to be directly observed.[3] Most importantly, the subsequent evolution of the radical-ion pair by a series of discrete steps to the ultimate ketonic products can be fully identified for the first time. In order to achieve this end, we exploit solvent and salt effects to probe the dynamic behaviour of [ESE$^{\bullet+}$, CA$^{\bullet-}$] in the context of the classical Fuoss–Winstein formulation of ion pairs over the extended time domain from picoseconds to microseconds.

Results

The spectral studies of the various reactive intermediates following the photoexcitation of chloranil were carried out by a series of pump-probe experiments in two distinct time regimes. In particular, the time-resolved spectroscopy focussed on the reactive intermediates formed in dichloromethane and acetonitrile solutions to represent the opposed extremes of solvent polarity, as earlier circumscribed by the product studies.[4]

The fastest picosecond studies for the temporal range from 0 to 4 ns utilized the 25 ps pulse[5] of monochromatic light at λ_{exc} = 355 nm (9 mJ per pulse) corresponding to the third harmonic output of a mode-locked (Quantel 501C-10) Nd: YAG laser.

The slower nanosecond/microsecond studies for the temporal range of 0–2000 μs were carried out with the third harmonic at 355 nm of the 10 ns pulse (22 mJ) from a Q-switched (Quantel 580-10) Nd: YAG laser in the ways described below.

The enol silyl ethers pertinent to the time-resolved spectroscopic studies were described in Part 1 and retain the same compound numbers in this paper (hence there are no compounds **1** and **8** in this paper).

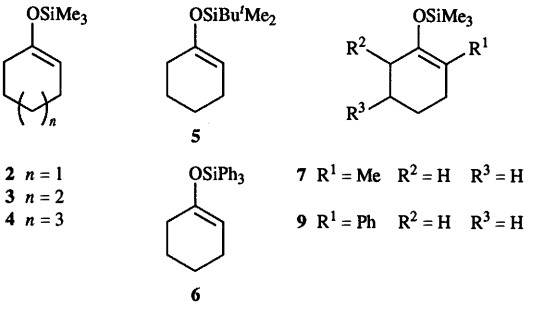

2 n = 1
3 n = 2
4 n = 3

5

6

7 R^1 = Me R^2 = H R^3 = H

9 R^1 = Ph R^2 = H R^3 = H

Picosecond spectral observation of the reactive intermediates in dichloromethane

Chloranil triplet (^{3}CA*). Upon the 355 nm (25 ps) excitation of chloranil dissolved in dichloromethane, the characteristic spectral band of the excited chloranil triplet was immediately observed. (The transient absorption spectrum of ^{3}CA* with λ_{max} = 510 nm was the same as that previously reported in acetonitrile,[6] butyronitrile[7] and 1,2-dichloroethane.[8]) The rise of this transient occurred on the same timescale of the 25 ps laser pulse, and the formation of ^{3}CA* was thus complete within 50 ps [eqn. (1)]. (The excited chloranil triplet ^{3}CA*

$$CA \xrightarrow[(<50\ ps)]{\lambda_{exc} = 355\ nm} {}^3CA^* \qquad (1)$$

formed under these conditions had a lifetime of $\tau = 5.6 \times 10^{-6}$ s.) Although the same transient with λ_{max} = 510 nm was also observed upon the 355 nm excitation of chloranil solutions containing equimolar amounts of various enol silyl ethers, the lifetime of ^{3}CA* was drastically reduced.

Chloranil anion radical (CA$^{\bullet-}$). Fig. 1A shows the rapid decay of the absorption band of ^{3}CA* in the presence of enol silyl

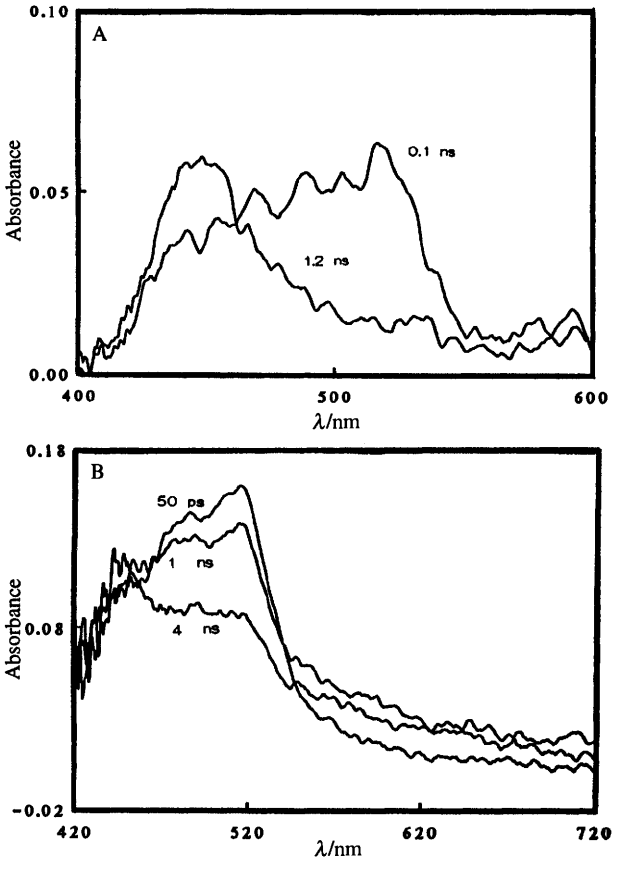

Fig. 1 (A) Time-resolved (picosecond) spectra from the quenching of ^{3}CA* by enol silyl ether **2** in dichloromethane, showing the spectral bands of chloranil triplet (λ_{max} = 510 nm) at 100 ps and chloranil anion radical (λ_{max} = 450 nm) at 1200 ps following the 355 nm laser pulse. (B) Same as (A) but with enol silyl ether **9**, showing the absorption tail of the cation radical **9**$^{\bullet+}$ in the spectral region from 550 to 700 nm.

ether **2**. The concomitant growth of the absorption band of chloranil anion radical CA$^{\bullet-}$ was apparent within 1.2 ns by its characteristic absorption band at λ_{max} = 450 nm[9] with an extinction coefficient of ε_{max} = 9600 dm^3 mol^{-1} cm^{-1}.[10] The transient quantum yield for the formation of CA$^{\bullet-}$ was estimated by comparing its absorbance at 450 nm (extrapolated to t = 0) with the absorbance of ^{3}CA* at 510 nm, also extrapolated to zero time. Quantum yields were calculated as $\Phi_{CA^{\bullet-}} = (A_{450}/A_{510})(\varepsilon_{3CA}/\varepsilon_{CA^{\bullet-}})$ and they are listed in Table 1. In view of the fact that both the chloranil triplet and the anion radical were both decaying on the picosecond timescale, the measured values of $\Phi_{CA^{\bullet-}}$ were subject to considerable error (± 10%). Nonetheless, the results in Table 1 indicated that triplet chloranil was efficiently converted to the anion radical with quantum yields uniformly exceeding 0.9, by all the enol silyl ethers examined in this study.

Enol silyl ether cation radicals (ESE$^{\bullet+}$). The observation of CA$^{\bullet-}$ with the high quantum yields in Table 1 implied the concomitant oxidation of enol silyl ether. Unfortunately, the absorption bands of most cation radicals of enol silyl ethers (ESE$^{\bullet+}$) generally lay below 350 nm, and they were not routinely observable on the picosecond timescale.[11] The exception was the cation radical of the 2-phenyl-substituted enol silyl ether **9**$^{\bullet+}$ (λ_{max} = 530 nm and ε_{max} = 5000 dm^3 mol^{-1} cm^{-1}.[12] Indeed, the red-shifted absorbance (apparent beyond 550 nm in Fig. 1B) was consistent with the highly transient formation of **9**$^{\bullet+}$ from the quenching of the excited chloranil triplet with 2-phenylcyclohexanone enol silyl ether **9**.[13] We thus associate the observation of CA$^{\bullet-}$ (with the high quantum yields listed in Table 1) to the efficient quenching of ^{3}CA* by enol silyl ethers, as in eqn. (2).

Table 1 Rate constants for ion-pair decay in Phase I and quantum yields for the formation of chloranil anion radical

Enol silyl ether	k_I[a]/10^9 s^{-1}	R[b]	Quantum yield ($\Phi_{CA^{\bullet-}}$)[c] CH_2Cl_2	CH_3CN
2	1.9	0.26	1.0	1.0
5	0.78	0.32	0.9	1.0
6	0.38	0.32	1.0	1.0
7	2.4	0.07	0.9	1.0

[a] Rate constants for the decay of chloranil anion (CA$^{\bullet-}$) in the time interval from 1.0–4.0 ns upon quenching of ^{3}CA* with the silyl enol ethers in column 1. [b] Residual absorbance relative to the maximum absorbance of the chloranil anion radical. [c] Quantum yield for CA$^{\bullet-}$, determined as the difference between the absorbance of CA$^{\bullet-}$ (extrapolated to zero time) and the initial absorbance of the chloranil triplet. The quantum yield for radical-ion pair formation given as Φ_{RIP} = Φ_{CA-} is described in ref. 36.

$$\text{ESE} + {}^3\text{CA}^* \xrightarrow[CH_2Cl_2]{\tau < 1.2\ \text{ns}} \text{ESE}^{\bullet+}, \text{CA}^{\bullet-} \qquad (2)$$

Hydrochloranil Radical (HCA$^{\bullet}$). The spectral decay of chloranil anion radical derived from the quenching of the enol silyl ethers listed in Table 1 was further monitored from 1.0 ns to beyond 4 ns. Thus, Fig. 2A shows the spectral evolution of the chloranil anion radical (CA$^{\bullet-}$ with λ_{max} = 450 nm recorded at 1.2 ns) to the residual spectrum of the hydrochloranil radical (HCA$^{\bullet}$ with λ_{max} = 435 nm[14] recorded at 3.0 ns) following the application of the 25 ps laser pulse to an equimolar solution of chloranil and cyclohexanone enol ether **2** in dichloromethane. The temporal change monitored at 450 nm (as presented in the inset to Fig. 2A) clearly shows the spectral decay to a raised baseline. By contrast, Fig. 2B shows the decay of CA$^{\bullet-}$ derived from quenching with 2-methylcyclohexanone enol silyl ether **7** to only a slight (~ 5%) residual absorbance. For comparative purposes, the residual absorbance was quantitatively evaluated for the enol silyl ethers in Table 1 as the ratio (R) of the 450 nm absorbance, measured after 4 ns relative to that at the temporal maximum,[15] *i.e.* $R = A_{4\ ns}/A_{max}$. The different rate constants for the decay of CA$^{\bullet-}$ derived from chloranil and various enol silyl ethers were obtained from the spectral decays by fitting the absorbance changes at 450 nm to a first-order process, and the values of k_I so obtained are listed in Table 1. Such large magnitudes of k_I indicated that the initial transformation of the chloranil anion radical to the hydrochloranil radical proceeded *via* hydrogen transfer from within the radical–ion pair prior to ionic separation.[16] Since the ion pair involves the enol silyl ether moiety, the hydrogen transfer must also be associated with the production of α-enone [eqn. (3)]. Thus, the picosecond

$$\text{ESE}^{\bullet+}, \text{CA}^{\bullet-} \xrightarrow{k_I} \alpha\text{-Enone} + \text{HCA}^{\bullet}, \textit{etc.} \qquad (3)$$

dynamics involved in the partial destruction of the radical ion pair, as described in eqn. (3), represented the immediate (fastest) process leading to enone. As such, the initial decay of CA$^{\bullet-}$ by the first-order rate constant k_I in Fig. 2A will be referred to hereafter as Phase I of the ion–pair kinetics.

Picosecond observation of the radical–ion pairs in acetonitrile

The time-resolved picosecond studies of chloranil excitation in the more polar acetonitrile solutions yielded results similar to those described above, and the spectral band position (λ_{max} = 510 nm) of the 25 ps transient was the same as that of ^{3}CA* in dichloromethane.

Chloranil anion radical. When the laser irradiation was carried out in the presence of the enol silyl ether **2**, the spectral band of ^{3}CA* was gradually replaced by the 450 nm band of the

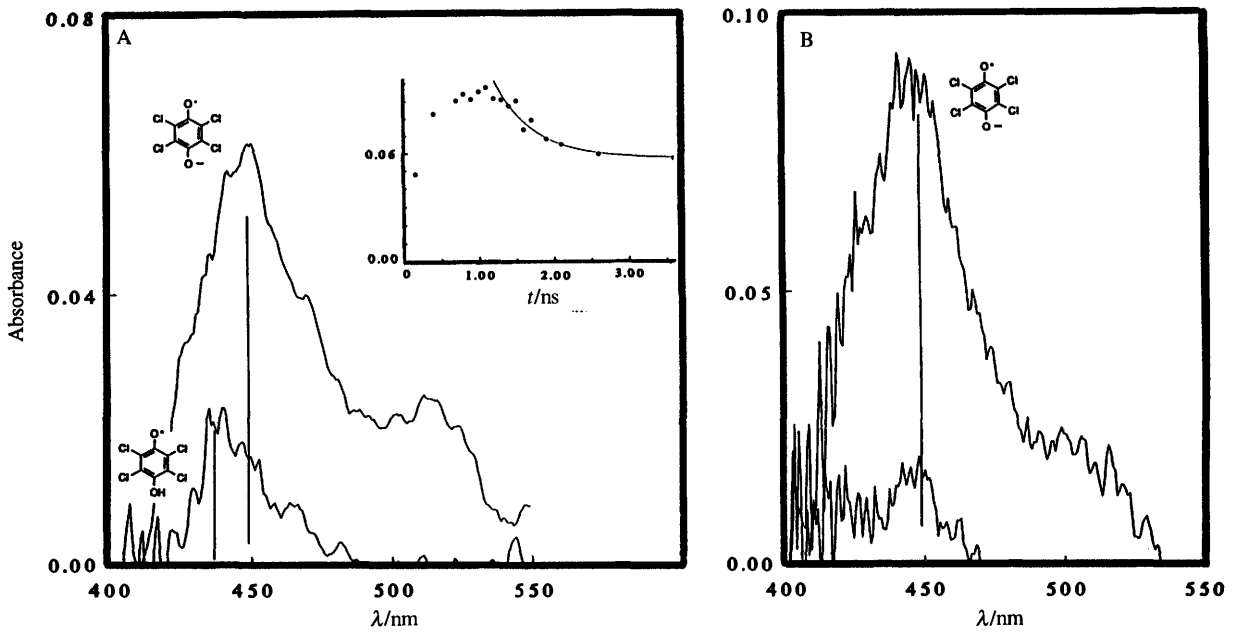

Fig. 2 (A) Temporal evolution of the transient spectrum of chloranil anion radical at t = 1.2 ns to the spectrum of hydrochloranil radical at t = 3.0 ns, following the quenching of ^{3}CA* by enol silyl ether **2** in dichloromethane. Inset: spectral decay (monitored at 450 nm) to a raised baseline and fitted to first-order kinetics. (B) Evolution of the spectrum of CA$^{\bullet -}$ from 0.3 ns to 3.0 ns, following the quenching of chloranil triplet by enol silyl ether **7** in dichloromethane.

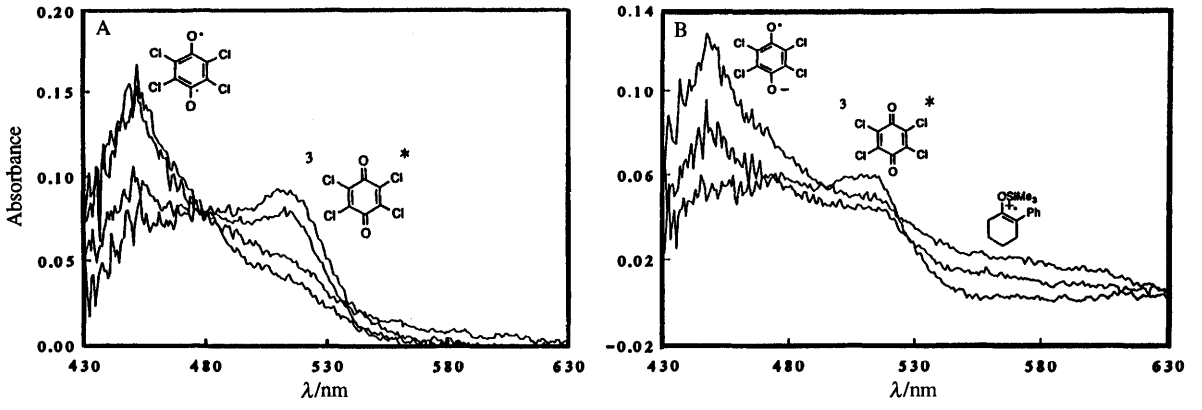

Fig. 3 (A) Decay of ^{3}CA* with λ_{max} = 510 nm and concomitant growth of chloranil anion radical (λ_{max} = 450 nm) upon the 355 nm excitation of chloranil in the presence of enol silyl ether **2** in acetonitrile. Spectra acquired at 100, 300, 500 and 1000 ps following the 25 ps laser pulse. (B) Same as (A), but measured with enol silyl ether **9** at 100, 800 and 1000 ps following the laser pulse. The low-energy spectral region clearly shows the growth of the cation radical **9**$^{\bullet +}$ between 550 and 600 nm.

chloranil anion radical; and Fig. 3A shows the progressive conversion of ^{3}CA* to CA$^{\bullet -}$ with a clear isosbestic point at λ = 480 nm. However, in contrast to the rapid subsequent decay of CA$^{\bullet -}$ in dichloromethane (*vide supra*), the spectral absorbance of CA$^{\bullet -}$ in acetonitrile persisted unchanged in intensity throughout the picosecond and nanosecond timescales.

Enol silyl ether cation radical. The longer lifetime of CA$^{\bullet -}$ in acetonitrile allowed the concurrent growth of the transient spectrum of the enol silyl ether cation radical **9**$^{\bullet +}$ to also be more clearly discerned in the spectral region beyond 530 nm (see Fig. 3B).[17] We thus conclude from the picosecond studies that the quenching of excited chloranil triplet by enol silyl ether **9** in acetonitrile resulted in the formation of the radical ion pair of CA$^{\bullet -}$ and **9**$^{\bullet +}$ on the same timescale (τ < 1.2 ns) as that described for dichloromethane (*vide supra*).

Hydrochloranil radical. Owing to the persistence of CA$^{\bullet -}$ in acetonitrile, the spectral region around λ_{max} = 435 nm for the hydrochloranil radical HCA$^{\bullet}$ was obscured for prolonged periods well beyond 4 ns. However, we judge from the high concentrations of CA$^{\bullet -}$ observed in Fig. 3A that HCA$^{\bullet}$ was formed in acetonitrile in only minor amounts, if at all.

Nanosecond kinetics of the formation and reactivity of the radical–ion pair in dichloromethane

The dynamics involved in the formation and destruction of the radical–ion pair, as described in eqns. (2) and (3), were also evaluated quantitatively on the nanosecond/microsecond timescale. For example, the 355 nm excitation of chloranil in dichloromethane with the longer 10 ns pulse from the Q-switched Nd:YAG laser afforded a transient absorption band with λ_{max} = 510 nm that was diagnostic of the excited chloranil triplet [see eqn. (1)]. (The spectral transient corresponding to ^{3}CA* persisted unchanged for ~500 ns and subsequently decayed by first-order kinetics with a rate constant of 1.8 × 10^5 s^{-1}.)

Formation of the radical–ion pair [ESE$^{\bullet +}$**, CA**$^{\bullet -}$**].** The lifetime of the excited chloranil triplet was dramatically reduced when cyclohexanone enol silyl **2** was present in solution, and Fig. 4 (inset) confirms the first-order decay of ^{3}CA*. Bimolecular rate constants for the quenching of ^{3}CA* by various enol silyl ethers (ESE) were determined by plotting the observed (pseudo) first-order rate constants against the concentration of the enol silyl ether.[18] A linear dependence was uniformly observed, and the values of the quenching rate constant k_q obtained from the slopes are listed in Table 2. The

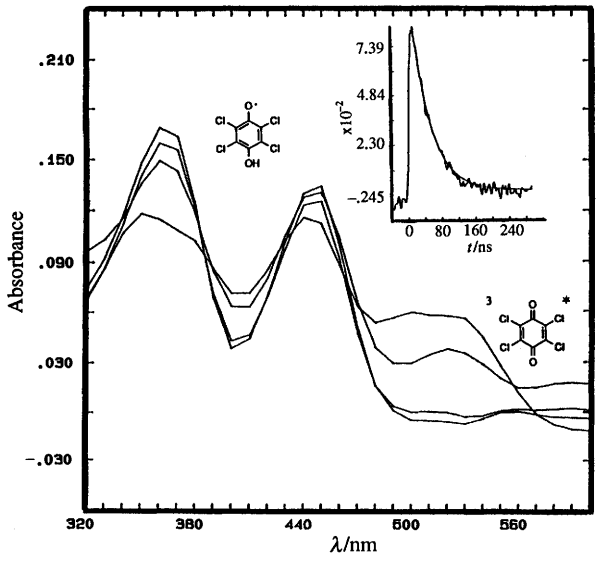

Fig. 4 Time-resolved (nanosecond) spectra acquired at 100, 140, 180 and 270 ns following the excitation of a dichloromethane solution of chloranil and enol silyl ether **2**. The spectral bands with λ_{max} = 370 and 435 nm belong to the hydrochloranil radical. Inset: spectral decay of ^{3}CA* monitored at 510 nm and its fit to first-order kinetics.

Table 2 Quenching rate constants (k_q) and transient quantum yields for hydrochloranil radical[a]

Enol silyl ether	k_q[b]/10^9 dm^3 mol^{-1} s^{-1}	Φ_{HCA}[c]
2	10	0.34
5	5.0	0.43
6	4.8	0.10
7	9.0	0.20
8	8.8	*d*
9	1.4	0.27

[a] Determined in dichloromethane solution at 23 °C. [b] From the observed pseudo-first-order rate constants *versus* silyl ether concentrations in the range (1.0–10.0) × 10^{-3} M. [c] Quantum yield for the formation of hydrochloranil radical determined by transient actinometry with benzophenone triplet as the actinometer. [d] Not determined.

Table 3 Quenching of various quinone triplets by cyclohexenyl trimethylsilyl ether in dichloromethane

Quinone	$E°_{red}$/V *vs.* NHE[a]	λ_{mon}(triplet)/ nm[b]	k_q/dm^3 mol^{-1} s^{-1}
Chloranil	+0.10	510	10 × 10^9
2,6-Dichloroquinone	−0.02	490	7.6 × 10^9
Benzoquinone	−0.16	430	1.2 × 10^8
Duroquinone	−0.50	490	3.0 × 10^7

[a] Reduction potential of the quinone (in aqueous solution) from Ref. 78. [b] Monitoring wavelength for the decay of the quinone triplet.

large magnitude and range of k_q = 0.5 to 1.0 × 10^{10} dm^3 mol^{-1} s^{-1} for the various cyclohexanone enol silyl ethers were indicative of the near diffusion-controlled quenching of ^{3}CA*. Moreover, the values of k_q in Table 2, together with the triplet lifetime of 5.8 μs (*vide supra*), indicated that the excited chloranil triplet was also completely quenched by enol silyl ethers under the preparative conditions described earlier.[4] The quenching rate constants progressively diminished when a series of less strongly oxidizing quinones were employed as photosensitizers for the oxidation of cyclohexanone enol silyl ether **2**.[19] The results in Table 3 show that k_q decreased in the order: chloranil > 2,6-dichloro-1,4-benzoquinone > 1,4-benzoquinone > duroquinone (tetra-methyl-1,4-benzoquinone)

Formation of hydrochloranil radical (HCA•). The characteristic spectrum of the chloranil triplet, when quenched by the various enol silyl ethers in Table 2, decayed to a residual spectrum consisting of twin bands at λ_{max} = 370 and 435 nm, as shown in Fig. 4.[20] This residual absorbance was readily identified as the absorption spectrum of the hydrochloranil radical (HCA•) on the basis of its identity with that previously described.[14,21–23] Since the transient spectrum of the hydrochloranil radical remained unchanged on the timescale of 200 to 500 ns, the quantum yield for HCA• was determined by the method of transient actinometry.[24] The triplet of benzophenone, generated by direct irradiation of benzophenone in benzene, served as the transient actinometer.[25] The actinometer solution and the solution of enol silyl ether and chloranil were irradiated side by side under identical conditions of ground-state absorbance and laser power, and the absorbances of the two solutions (λ_{BP} = 530 nm and λ_{HCA} = 435 nm) were compared. The quantum yields (Φ_{HCA}) for the formation of the hydrochloranil radical were determined from the relationship: $\Phi_{HCA} = (A_{435}/A_{530})\ (\varepsilon_{BP}/\varepsilon_{HCA})$, where ε_{BP} and ε_{HCA} are the extinction coefficients of the triplet state of benzophenone (ε_{BP} = 7220 dm^3 mol^{-1} cm^{-1} at 530 nm)[25] and the hydrochloranil radical (ε_{HCA} = 7700 at 435 nm),[14] respectively. It is important to note that the values of Φ_{HCA} significantly less than unity (Table 2) indicated a deficit in the amount of HCA• that could be spectrally observed on the nanosecond timescale. Moreover, comparison of the quantum yields for HCA• formation in Table 2 with those for silyl ether consumption (Φ_{loss}) and enone formation (Φ_{enone}) in Table 4 indicated that the hydrochloranil radical observed on the nanosecond and microsecond timescales could not have been the sole intermediate in the formation of enone. For example, the quantum yield of 0.68 for enone formation from cyclohexanone enol trimethylsilyl ether (**2**) was two times higher than the quantum yield of 0.34 for the (measured) formation of hydrochloranil radical. In other words, the time-resolved nanosecond studies clearly revealed the discrepancy that generally existed between Φ_{enone} (Table 4) and Φ_{HCA} (Table 2). This, coupled with the high quantum yield for the formation of CA•$^-$ (Table 1), must indicate the presence of another pathway(s) leading to the enone, in addition to that posed by the picosecond studies in eqn. (3).

Table 4 Quantum yields for the loss of enol silyl ether and the formation of enone[a]

Enol silyl ether	Solvent	Quantum yields Φ_{loss}[b]	Φ_{enone}[c]	Φ_{adduct}[d]
2	CH_2Cl_2	0.83	0.68	0.15
	CH_3CN	0.79	0.04	0.75
3	CH_2Cl_2	0.68	0.03	0.65
4	CH_2Cl_2	0.65	0.01	0.64
5	CH_2Cl_2	0.87	0.63	0.24
	CH_3CN	0.90	0.72	0.18
6	CH_2Cl_2	0.35	0.28	0.07
	CH_3CN	0.50	0.48	0.02
7	CH_2Cl_2	0.08	0.07	0.01
	CH_3CN	0.09	0.01	0.08
9	CH_2Cl_2	0.05	0.04	0.01

[a] From the irradiation (λ = 360 ± 10 nm) of equimolar solutions of chloranil and enol silyl ether (0.02 M) taken from Ref. 1. Photon fluxes were determined with potassium ferrioxalate as actinometer. [b] Quantum yields for the conversion of silyl enol ether (±0.07). [c] Quantum yields for enone formation (±0.05). [d] Quantum yields for adduct formation calculated on the basis of ($\Phi_{loss} - \Phi_{enone}$).

Transient (nanosecond) behaviour of the radical–ion pair in acetonitrile

The absorption spectrum of the chloranil anion radical (CA•$^-$) was the prominent feature of the time-resolved study of the quenching of the excited chloranil triplet by cyclohexanone enol

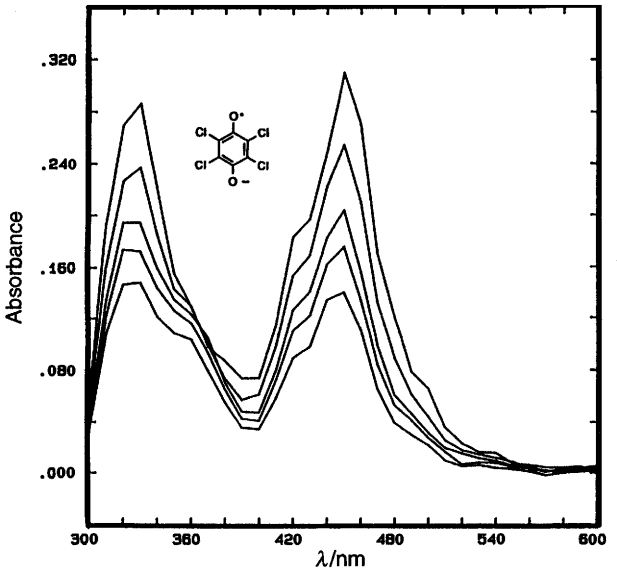

Fig. 5 Spectral decay of chloranil anion radical on the microsecond timescale at t = 0.5, 9.3, 1.8, 2.7 and 4.5 μs following the quenching of ^{3}CA* with enol silyl ether **2** in acetonitrile

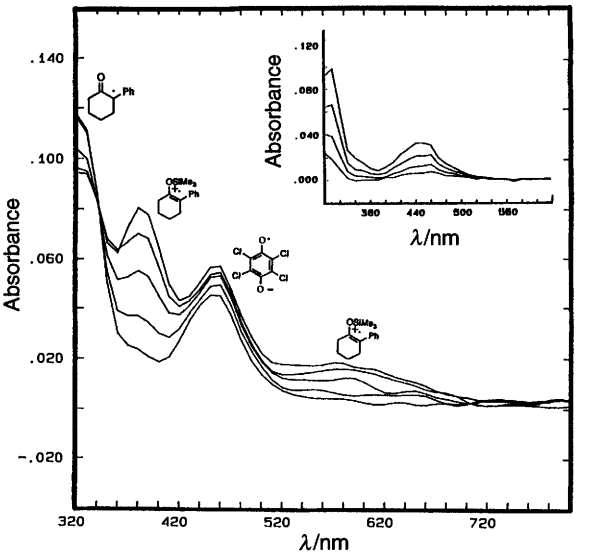

Fig. 6 Time-resolved (nanosecond) spectra obtained at t = 0.36, 0.44, 0.60, 0.92 and 1.56 μs after the 355 nm excitation of chloranil in the presence of enol silyl ether **9** in acetonitrile, showing the spectral decay of cation radical $\mathbf{9}^{\bullet+}$ and the concomitant growth of the desilylated radical (α-phenylcyclohexanonyl). Inset: simultaneous spectral decay of the desilylated radical and chloranil anion radical recorded at t = 45, 61, 92 and 156 μs.

silyl ether in acetonitrile with the 355 nm (10 ns) laser pulse. Most importantly, Fig. 5 shows the well resolved visible band at λ_{max} = 450 nm, together with the UV band at λ_{max} = 330 nm of $CA^{\bullet-}$.[10] Thus, Fig. 5 was in strong contradistinction to Fig. 4 which features the prominent spectrum of the hydrochloranil radical obtained in dichloromethane solution, under otherwise the same conditions. (Note that $HCA^{\bullet}$ is absent, or at best, only a minor constituent in Fig. 5.) In further contrast, the spectral absorbance of $CA^{\bullet-}$ generated in acetonitrile remained unchanged in intensity throughout the picosecond and nanosecond time regimes; and it finally decayed slowly to the spectral baseline by second-order kinetics on the microsecond timescale with a rate constant of $k_2 \approx 10^{10}$ dm^3 mol^{-1} s^{-1}.

The accompanying behaviour of the enol silyl ether cation radical ($ESE^{\bullet+}$) in acetonitrile solution could also be examined on the nanosecond timescale with the 2-phenyl analogue $\mathbf{9}^{\bullet+}$ (compare the picosecond spectra in Fig. 3B). Thus, the excited chloranil triplet was completely quenched by 2-phenylcyclohexanone enol silyl ether (**9**) within 20 ns of the 10 ns laser pulse. Fig. 6 shows the broad visible band of $\mathbf{9}^{\bullet+}$ centred at ~540 nm,[12] together with that of $CA^{\bullet-}$ at λ_{max} = 450 nm. In the high energy portion of the spectrum, the UV band of $\mathbf{9}^{\bullet+}$ was observed at λ_{max} = 370 nm,[26] together with that of $CA^{\bullet-}$ (which appears as a spectral tail). The absorption bands of $\mathbf{9}^{\bullet+}$ at λ_{max} = 540 and 370 nm decayed simultaneously by first-order kinetics with $k_{ESE^{\bullet+}} = 1.7 \times 10^7$ s^{-1}. A new transient ascribed to the 2-phenylcyclohexanonyl radical with a UV absorption at $\lambda_{R^{\bullet}} \approx 320$ nm[27] grew simultaneously, eqn. (4).[28]

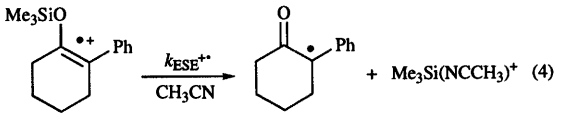

On this submicrosecond timescale, the absorption spectrum of the chloranil anion radical was unchanged. However, it subsequently decayed by second-order kinetics, with the rate constant $k_2 = 9.6 \times 10^{10}$ dm^3 mol^{-1} s^{-1} evaluated from the extinction coefficient of $CA^{\bullet-}$ of 9600 dm^3 mol^{-1} cm^{-1} at 450 nm.[10]

Salt effect on the transient behaviour of chloranil anion radical

The role of the ionic environment around the radical-ion pair [$ESE^{\bullet+}$, $CA^{\bullet-}$] was examined by the deliberate addition of the neutral salt tetrabutylammonium hexafluorophosphate ($TBA^+PF_6^-$) to the dichloromethane solution of chloranil and cyclohexanone enol silyl ether **2**. The temporal behaviour of the radical–ion pair was spectrally monitored by observing the changes in the chloranil anion radical in two time regimes as follows.

Picosecond dynamics in the temporal range: 1–4 ns. The temporal effect of added salt on the decay profile of the chloranil anion radical at λ_{max} = 450 nm was initially examined on the fastest picosecond timescale, utilizing the 25 ps (355 nm) laser pulse. Significantly, the presence of small amounts of $TBA^+PF_6^-$ (*e.g.* 0.5 to 5.0 × 10^{-4} M) had no measurable effect on the decay kinetics of $CA^{\bullet-}$ in the time interval from 1 to 4 ns that was earlier defined by the temporal profile shown in the inset to Fig. 2A.

Nanosecond dynamics in the temporal range: 10–200 ns. The temporal effect of added salt on $CA^{\bullet-}$ was next examined on the slower nanosecond/microsecond timescale, allowed by the more extended 10 ns (355 nm) laser pulse. Fig. 7A shows the temporal behaviour of $CA^{\bullet-}$ that was detected by monitoring the absorbance change at λ_{mon} = 480 nm.[29] Thus, the spectral decay in the time period from 10 to 200 ns to the raised baseline in Fig. 7A represented the first-order kinetics for Phase II of the disappearance of $CA^{\bullet-}$ (with $k_{II} = 2.2 \times 10^7$ s^{-1}) that occurred subsequent to the initial decay observed on the picosecond timescale (Phase I) in Fig. 2A. The decay in Phase II, unlike Phase I, was extremely sensitive to the presence of added (inert) salt, since as little as 5.0 × 10^{-4} M $TBA^+PF_6^-$ was sufficient to eliminate it completely. Dramatically, the decay was replaced by an enhanced absorbance in Fig. 7B, which did not undergo further change on this timescale. Additional increments of salt led to a gradual elevation of the absorbance plateau (see Fig. 7C).

The salt effect could be quantified by the determination of the quantum efficiency for the formation of $CA^{\bullet-}$ at various concentrations of added $TBA^+PF_6^-$. The absorbance of $CA^{\bullet-}$ was consistently measured at 480 nm on the temporal plateau attained in the 100–800 ns timescale.[29b] The quantum yield of $CA^{\bullet-}$ is plotted as Φ_{CA^-} in Fig. 8 as a function of added salt. Thus, as the concentration of $TBA^+PF_6^-$ increased, the quantum yield of $CA^{\bullet-}$ increased monotonically, but with a sharp non-linear increase in Φ_{CA^-} of 0.01 to 0.08 at relatively low concentrations (< 2 × 10^{-3} M) of added salt (see inset).

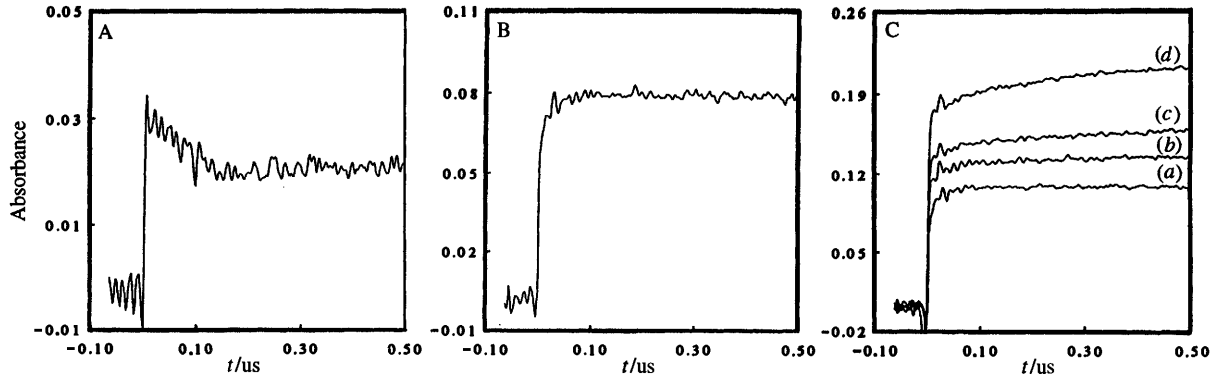

Fig. 7 Spectral traces for chloranil anion radical monitored at 460 nm upon the quenching of chloranil triplet by enol silyl ether **2** in dichloromethane containing (A) no added salt and (B) in the presence of 5.0×10^{-4} M $TBA^+ PF_6^-$. (C) Same as (A) but containing (*a*) 3.0, (*b*) 8.3, (*c*) 11.0 and (*d*) 19.0 $\times 10^{-3}$ M $TBA^+ PF_6^-$

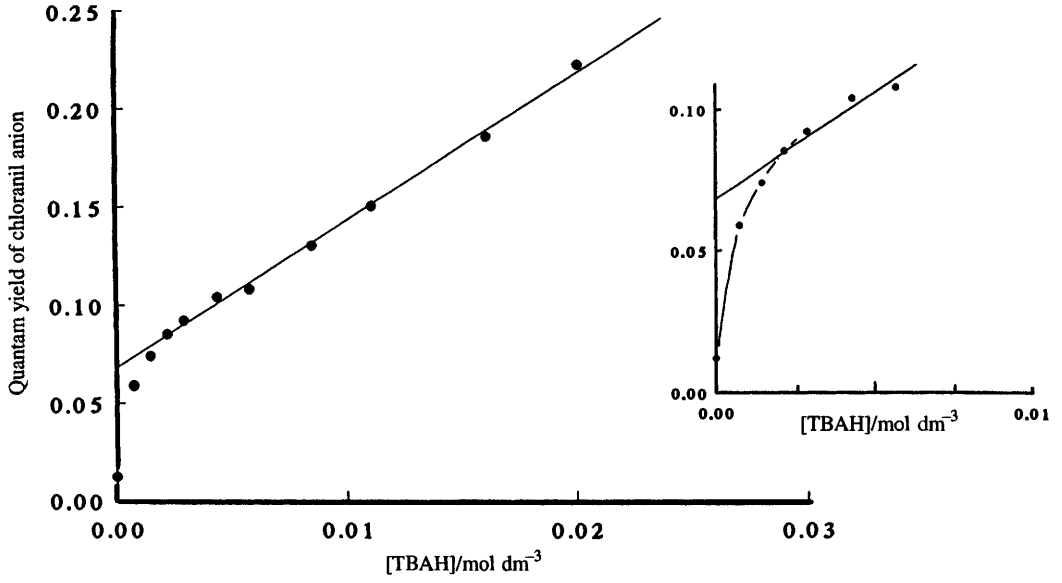

Fig. 8 Variation in the quantum yield for the formation of chloranil anion radical during the quenching of ^{3}CA* with enol silyl ether **2** in dichloromethane containing increasing amounts of $TBA^+PF_6^-$. Inset: enlargement of the plot at low salt concentrations of < 0.01 M.

This was followed by a gradual, linear increase of $\Phi_{CA^{\cdot-}}$ at higher salt concentrations. At the highest concentration of added salt, the spectral band of hydrochloranil radical (see Fig. 4) was completely replaced by the characteristic absorption spectrum of chloranil anion radical with λ_{max} = 450 and 330 nm.[10]

Discussion

Time-resolved spectroscopy over two time domains from picoseconds to nanosecond/microsecond allows the temporal evolution of the various intermediates involved in the oxidative elimination and addition of enol silyl ethers by photoactivated chloranil to be serially observed in the following way.

Electron-transfer quenching and formation of the radical–ion pair

The triplet absorbance of chloranil is effectively quenched by enol silyl ether **2** at near diffusion-controlled rates (see Table 2). The decay of ^{3}CA* in both dichloromethane and acetonitrile is accompanied by the simultaneous growth of the chloranil anion radical ($CA^{\cdot-}$), as shown in Figs. 1 and 3.[30] This observation, combined with the quantum-efficient formation of $CA^{\cdot-}$ in Table 1, leads to the conclusion that the quenching of triplet chloranil occurs by way of electron transfer to form the radical–ion pair as in eqn. (5).[31] The cation radical of enol silyl ether **9** is

$$ESE + {}^3CA^* \xrightarrow[(\Phi_{RIP})]{k_q} ESE^{\cdot+}, CA^{\cdot-} \qquad (5)$$

directly observed as a spectral transient, and Fig. 3B shows the absorption band of $9^{\cdot+}$ rising concurrently with that of $CA^{\cdot-}$ (and concomitant decay of ^{3}CA*), as demanded by the stoichiometry in eqn. (5).[36] Such a direct observation of the electron-transfer quenching in dichloromethane, as well as in acetonitrile, demonstrates that the formation of the radical–ion pair is the initial step that subsequently results in both the oxidative elimination and addition pathways (Scheme 1).

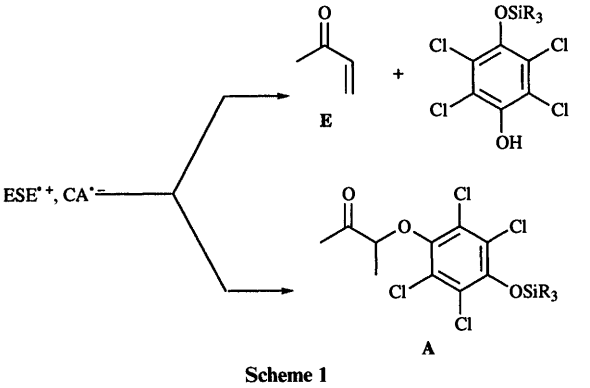

Scheme 1

Electron transfer is energetically favoured for enol silyl ethers generally, since chloranil in its excited triplet state is a powerful electron acceptor, with E°_{red} = +2.15 V *vs.* SCE,[37] and enol silyl ethers are oxidized at potentials between 1.0 and 1.5 V.[41]

Thus a positive driving force of $-\Delta G_{ET}$ = 13–22 kcal mol^{-1}† can be estimated for the radical–ion pair formation in eqn. (5). If this driving force is diminished by choosing a quinone with a lower redox potential as the photosensitizer, the quenching rate drops and no photochemical reaction results (Table 3). For example, changing the sensitizer from chloranil to duroquinone in the reaction with enol silyl ether **2** reduces the driving force from 15 to 3 kcal mol^{-1}, and the quenching rate constant drops by a factor of 300. The electron transfer in eqn. (5) is also consistent with the facile formation of a series of related radical–ion pairs [D$^{\bullet+}$ CA$^{\bullet-}$] when ^{3}CA* is quenched with a variety of aliphatic and aromatic donors (D).[7–9,32–34]

Microdynamics of contact ion pairs: internal return *versus* solvent separation

The radical ion pairs [ESE$^{\bullet+}$, CA$^{\bullet-}$] are formed with unit quantum yield in both dichloromethane and acetonitrile (Table 1), but their subsequent reactions are very different in the two solvents. In dichloromethane, the contact radical–ion pair decays on the early nanosecond timescale (with k_I = 1.9 × 10^9 s^{-1}) to afford the hydrochloranil radical HCA$^{\bullet}$ Thus, the predominant decay process is identified as the deprotonation of 2$^{\bullet+}$ by the anion radical of chloranil (CA$^{\bullet-}$). In other words, the critical step leading to enone formation is the collapse of the ion pair *via* an interionic proton transfer (k_{PT}) [eqn. (6)]. Proton

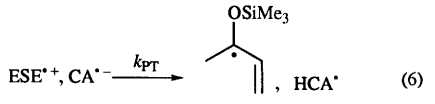

(6)

transfer within contact ion pairs has been inferred in a variety of other photoinduced electron transfers,[42–44] and the chloranil anion radical is a sufficiently strong base for proton removal from arene radical cations.[8,45] The quantitative assessment of the energetics of the proton transfer in eqn. (6) is not possible at this juncture (owing to the unknown values of pK_A for enol silyl ether cation radicals). However, it should be noted that cation radicals of simple alkenes are strong Brønsted acids, and they are readily deprotonated by weak bases such as alcohols.[46,47]

Since the ion pair collapse in eqn. (6) represents the internal return of the contact ion pair according to the Winstein scheme for ion pairing,[50] the distinction between contact (or intimate) and solvent-separated ion pairs[51–55] must be explicitly taken into account [eqn. (7)].

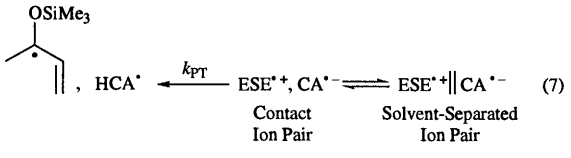

(7)

The contact ion pairs (CIP) and solvent-separated ion pairs (SSIP) are related according to the general Winstein formulation in eqn. (7), and they can be distinguished by their contrasting response to added inert salt.[56] In particular, an inert salt (M$^+$ X$^-$) undergoes rapid exchanges with the contact ion pair [eqn. (8)], as well as with the solvent-separated ion

$$ESE^{\bullet+}, CA^{\bullet-} + M^+, X^- \rightleftharpoons M^+, CA^{\bullet-} + ESE^{\bullet+}, X^- \quad (8)$$

pair. Since the individual ions ESE$^{\bullet+}$ and CA$^{\bullet-}$ become separated in eqn. (8), the internal return processes in eqn. (6) are precluded. Solvent separated ion pairs are effectively scavenged at low concentrations of salt (*ca.* 10^{-3} M), while contact ion pairs require substantially higher salt concentrations to effect separation.[57,58] When the scavenging efficiency is plotted against the salt concentration, a biphasic behaviour results—an abrupt increase in the yield of scavenged ions at low concentrations (special salt effect) corresponding to the interception of the solvent-separated ion pairs,[58–60] and a linear region at higher salt concentrations, corresponding to the exchange of the contact ion pair.[56] For the ion pairs formed *via* electron transfer quenching in eqn. (5), the fraction of scavenged chloranil anion radical (Φ_{CA^-}) can be directly determined and quantified by time-resolved spectroscopy. The initial non-linear rise in the plot of Φ_{CA^-} *versus* added salt in Fig. 8 is diagnostic of the special salt effect[58,60] and indicates the scavenging of the solvent-separated ion pairs (2$^{\bullet+}$ || CA$^{\bullet-}$) by added salt. The quantum yield of solvent-separated ion pairs in dichloromethane is obtained from the plot in Fig. 8 as the difference between the quantum yield for CA$^{\bullet-}$ formation (extrapolated to zero from the linear portion of the plot) and the quantum yield of CA$^{\bullet-}$ at zero salt concentration. A value of Φ_{SSIP} = 0.06 is obtained. Since the quantum yield for the formation of ion pairs is unity (see Table 1), the low value of Φ_{SSIP} indicates that the predominant ion pair formed in dichloromethane [eqn. (5)] is the contact ion pair. Moreover, the rapidity of this reaction, combined with the limited quantum yield for separation of the ions, leads to the conclusion that proton transfer occurs within the contact radical–ion pair prior to the solvent separation steps in eqn. (7).[61]

In sharp contrast to the rapid ion-pair collapse observed in non-polar dichloromethane, the ion pairs [2$^{\bullet+}$, CA$^{\bullet-}$] formed in acetonitrile undergo diffusive separation. No decay of CA$^{\bullet-}$ is observed on the picosecond or nanosecond timescales, and the subsequent decay of CA$^{\bullet-}$ on the microsecond timescale, occurs by second-order kinetics. Such bimolecular (second-order) decays are characteristic of the recombination of free ions.[52,62] Proton transfer within the contact radical–ion pair does not compete in this solvent, as shown by the absence of the absorption band of hydrochloranil radical (HCA$^{\bullet}$) in the transient spectra (compare Figs. 4 and 5), and the low yield of enone in Table 4. Therefore, the crucial step in the oxidative addition pathway is the separation of the radical–ion pair to form free ions.[63] The effect of inert salt in diverting the reaction from oxidative elimination to oxidative addition[64] can similarly be ascribed to the *induced* separation of the contact ion pair by added salt [M$^+$X$^-$ in eqn. (8)].[65]

The branching point in the two processes of elimination and addition in Scheme 1 are identified as the competition between solvent separation (k_{SEP}) and interionic proton transfer (internal return, k_{PT}) in Scheme 2. Such a competition has been

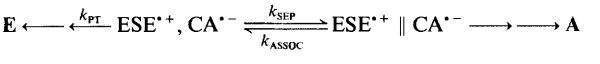

Scheme 2

previously delineated in time-resolved studies of ion pairing, and the effects of increasing solvent polarity to facilitate the separation of contact ion pairs have been identified.[54]

Subsequent reactions of the radical intermediates: elimination and addition

Oxidative elimination. Proton transfer within the radical–ion pair in eqn. (6) yields a pair of neutral radicals which undergoes diffusive separation (*i.e.* cage escape). The quantum yield of freely diffusing radicals (Φ_{diff}) is given simply by the quantum yield of the hydrochloranil radical determined on the nanosecond timescale, as given by Φ_{HCA} in Table 2. Since this value is less than the quantum yield for enone formation in Table 4, we conclude that at least some of the enone is formed prior to the diffusive separation of the radical pair. In other words, radical-pair collapse to yield enone and hydrochloranil trimethylsilyl ether competes with the radical-pair separation (Scheme 3). According to Scheme 3, oxidative elimination occurs both by (i) geminate recombination (k_{gem}) of the radical

† 1 cal = 4.184 J.

Table 5 Rate constants for ion-pair microdynamics of [ESE$^{\bullet+}$, CA$^{\bullet-}$] contact ion pairs

Fate of the contact ion-pair	Φ^a	$k^b/10^9$ s^{-1}
Proton Transfer (PT)	0.68	1.2
Solvent Separation (SEP)	0.06[c]	0.11
Back Electron Transfer (BET)	0.20	0.36

[a] Derived from the steady-state quantum yields in Table 4, taken as: $\Phi_{PT} = \Phi_{enone}$, and $\Phi_{BET} = 1 - \Phi_{loss}$. [b] Calculated as $k = \Phi k_I$ for each of the processes in column 1. [c] From the special salt effect in Fig. 8, see text.

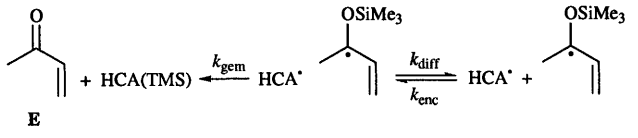

Scheme 3

pair in eqn. (7) (formed by ion-pair collapse in Scheme 2) and (ii) diffusive separation (k_{diff}), followed by the encounter of the freely diffusing radicals (k_{enc}). The relative contribution of the two processes can be estimated as follows: the quantum yield of enone (Φ_{enone} in Table 4) is equal to the quantum yield of radical pairs formed by proton transfer, and both must be equal to the sum of geminate recombination (Φ_{gem}) and cage escape processes (Φ_{diff}). For the enol silyl ether **2**, the quantum yields for Φ_{enone} and Φ_{diff}, are 0.68 and 0.34, respectively, and thus the quantum yield for geminate recombination Φ_{gem} is 0.34. Thus, cage escape and geminate recombination occur with more or less equal probability.[66]

Oxidative addition. The radical cation of the trimethylsilyl enol ether derived from 2-phenylcyclohexanone undergoes loss of trimethylsilyl cation in acetonitrile solution [eqn. (4)]. Such a desilylation is likely to be general for enol silyl ether radical cations, and would then occur with a rate constant k_{deSi} of approximately 10^7 s^{-1} in this solvent. Indeed, enol silyl ether radical cations are known to undergo loss of the silyl group in methanol,[67] and the loss of silyl substituents from aromatic cation radicals is well known.[68] The products of this reaction are the (solvated) trimethylsilyl cation and the α-ketoalkyl radical.[69] The latter reacts rapidly with CA$^{\bullet-}$ by a second-order (radical–radical) combination, and the subsequent (fast) transfer of the silyl cation to the anionic intermediate yields the adduct, as illustrated in Scheme 4.

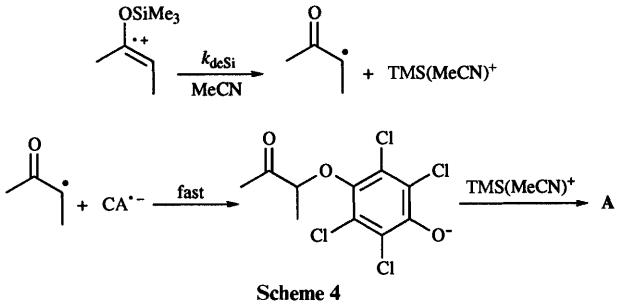

Scheme 4

The general features of oxidative elimination in Scheme 3 and oxidative addition in Scheme 4 accord with the predominance of free-radical processes in non-polar solvents such as dichloromethane in Scheme 3, and of ionic processes in more polar environments such as acetonitrile in Scheme 4. The dichotomy between oxidative elimination and addition thus can be directly traced to the branching of the reaction pathways at the contact ion-pair stage, as depicted in Scheme 2.

Back electron transfer within the contact radical–ion pair

Although the quantum yield for the oxidative conversion of enol silyl ether **2** is high ($\Phi_{loss} = 0.80$ in Table 4), it is less than unity. Since the formation of the contact radical–ion pair occurs with unit efficiency (Table 1), there must be a minor process, such as back electron transfer,[31b] that returns the contact ion pair [CA$^{\bullet-}$, **2**$^{\bullet+}$] to the starting materials [eqn. (9)]. Back

$$\text{ESE}^{\bullet+}, \text{CA}^{\bullet-} \xrightarrow{k_{BET}} \text{ESE} + \text{CA} \qquad (9)$$

electron transfer (BET) is commonly observed in photoinduced electron transfers, and has been the subject of a variety of time-resolved spectroscopic studies.[70–72] The efficiency of BET is simply given by the difference between Φ_{RIP} in Table 1 and the quantum yield for silyl enol ether conversion (Φ_{loss}) in Table 4. For the enol silyl ether **2**, this difference yields a value of $\Phi_{BET} = 0.20$ in dichloromethane and 0.10 in acetonitrile. Scheme 2 must thus be modified to take into account such an energy-wasting back electron transfer (Scheme 5). According to

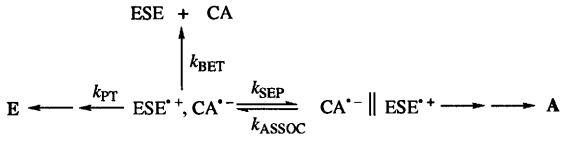

Scheme 5

Scheme 5, the contact ion pair is subject to three simultaneous microdynamical processes, namely proton transfer (PT), solvent separation (SEP) and back electron transfer (BET). The overall ion-pair decay is represented by the composite (observed) rate constant [k_I in eqn. (3)], which is the sum of the rate constants ($k_{PT} + k_{SEP} + k_{BET}$). The relative contributions of these microdynamical processes in Scheme 5 is given by the quantum yields in Table 4 and the special salt effect (*vide supra*). The rate constants evaluated as $k_{PT} = \Phi_{PT}k_I$, $k_{SEP} = \Phi_{SEP}k_I$ and $k_{BET} = \Phi_{BET}k_I$ are listed in Table 5. In the absence of free-ion formation (*e.g.* in dichloromethane), the rate constant for (re)association of the solvent-separated ion pair to the contact ion pair is given by k_{II}, the rate constant for the nanosecond (Phase II) decay of CA$^{\bullet-}$. This yields a value of $k_{ASSOC} = 2.2 \times 10^7$ s^{-1}.[73]

In acetonitrile, the ion-pair separates quantitatively to free ions, so that k_{SEP} is much greater than either k_{BET} or k_{PT} in this solvent. The small amount of back electron transfer ($\Phi_{BET} = 0.10$) and proton transfer ($\Phi_{PT} = \Phi_{enone} = 0.04$) occurs by re-formation of the contact radical–ion pair. This bimolecular process is slow compared with the desilylation in Scheme 4, as shown by the high yields of adduct in Table 4.

Mechanistic consequences of ion-pair dynamics on product formation

The competition between ion-pair separation and internal return in Scheme 2, coupled with the follow-up reactions in Schemes 3 and 4 constitute the principal pathways by which enone and adduct are formed from enol silyl ether and photoexcited chloranil. The minor pathway of back electron transfer is also identified in eqn. (9). Accordingly, let us consider how these processes explain the varied photochemistry of the enol silyl ethers. The structural effects of the silyl enol ether donors can be identified in terms of (i) the effect of ring size, (ii) the effect of the silyl leaving group and (iii) the effect of alkyl substitution. It should be noted that the formation of the ion-pair in Table 1 occurs efficiently for all silyl enol ethers, as evidenced by the high values of k_q in Table 2 and the unit quantum efficiency for radical–ion pair formation (Φ_{RIP}) in Table 1. Therefore, the critical steps in accounting for the effects identified above must occur after the electron-transfer quenching in eqn. (5), and therefore reflect the ion-pair dynamics in Scheme 2 in the following way.

Ring size. The enol silyl ethers (**3** and **4**) derived from seven- and eight-membered ring ketones react by oxidative addition

even in the non-polar dichloromethane.[4] Since solvent separation is unlikely to be markedly faster for these substrates than for the cyclohexane analogue (**2**), the high yields of adduct must reflect a lower rate of proton transfer. Such a retardation can arise from a structural change in the enol silyl ether cation radical, as follows. Alkene cation radicals with oxy-substituents (such as those derived from enol silyl ethers) can be transformed into the distonic form by twisting around the double bond, as shown in structures **I** and **II**. The dihedral angle around the

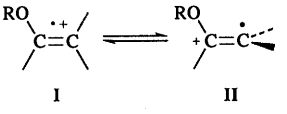

I **II**

double bond is calculated to be 1.8 and 22° for $\mathbf{2}^{\bullet+}$ and $\mathbf{3}^{\bullet+}$, respectively. In other words, the six-membered ring is calculated to have an untwisted double bond and hence the charge in $\mathbf{2}^{\bullet+}$ is delocalized (**I**),[74] but the seven-membered analogue $\mathbf{3}^{\bullet+}$ has appreciable distonic character. Localization of the positive charge in **II** is expected to result in decreased acidity of the cation radical (as it begins to resemble a carbon-centred radical). (Moreover, the positive charge adjacent to the silyl group in **II** will facilitate desilylation.) As a result of these effects, the enol silyl ether cation radicals $\mathbf{3}^{\bullet+}$ and $\mathbf{4}^{\bullet+}$ are expected to preferentially undergo solvent separation (followed by desilylation) rather than deprotonation.

Silyl leaving group. Since the loss of the silyl cation is a critical step in the formation of adducts according to Scheme 4, the effects of alkyl substitution on the silyl group must be taken into account. Although the relative rates of desilylation for the various R_3Si-substituted cation radicals is not known, *tert*-butyldimethylsilyl- and triphenylsilyl-substituted enol ethers are much more stable to acidic hydrolysis than their trimethylsilylated analogues.[75] If the same trend applies to the solvolytic loss of R_3Si^+ in Scheme 4, the cation radicals $\mathbf{5}^{\bullet+}$ and $\mathbf{6}^{\bullet+}$ are expected to react more slowly than $\mathbf{2}^{\bullet+}$ The reduced rates of desilylation for these radicals will allow the re-formation of the contact radical ion pair as in eqn. (10) and thus

$$ESE^{\bullet+} + CA^{\bullet-} \rightleftharpoons [ESE^{\bullet+}, CA^{\bullet-}] \qquad (10)$$

enhance ion-pair collapse and enone formation according to Schemes 2 and 3. The net effect is to favour oxidative elimination even under conditions (acetonitrile solvent) in which ion-pair separation occurs efficiently.

Alkyl substitution. A high quantum yield for ion-pair formation upon the quenching of the 2-methyl-substituted enol silyl ether (**7**) in Table 1 does not translate into a high overall quantum yield for the reaction (Φ_{loss} = 0.07 in Table 4). The discrepancy between Φ_{RIP} and Φ_{loss} is attributed to efficient back electron transfer in the radical–ion pair, as discussed for eqn. (9). Back electron transfer from the 2-substituted enol silyl ether cation radicals ($\mathbf{7}^{\bullet+}$ and $\mathbf{9}^{\bullet+}$) is substantially less exothermic than BET from the unsubstituted analogues.[1] According to recent studies,[70–72] the reduced driving force is associated with increased rates of back electron transfer.[76] Thus the decay of $CA^{\bullet-}$ to a small residual of $HCA^{\bullet}$ in Fig. 2B is consistent with predominant back electron in the radical–ion pair [$\mathbf{7}^{\bullet+}$, $CA^{\bullet-}$].

Conclusions

Exploitation of time-resolved spectroscopy, particularly with regard to the solvent and salt effects, allows the full course of the photoinduced electron transfer of enol silyl ethers with quinone to be directly observed. Picosecond studies establish the formation of α-enones to be initiated by electron-transfer quenching of the silyl enol ether donor by chloranil in its excited triplet state to generate the contact radical ion pair (CIP), as

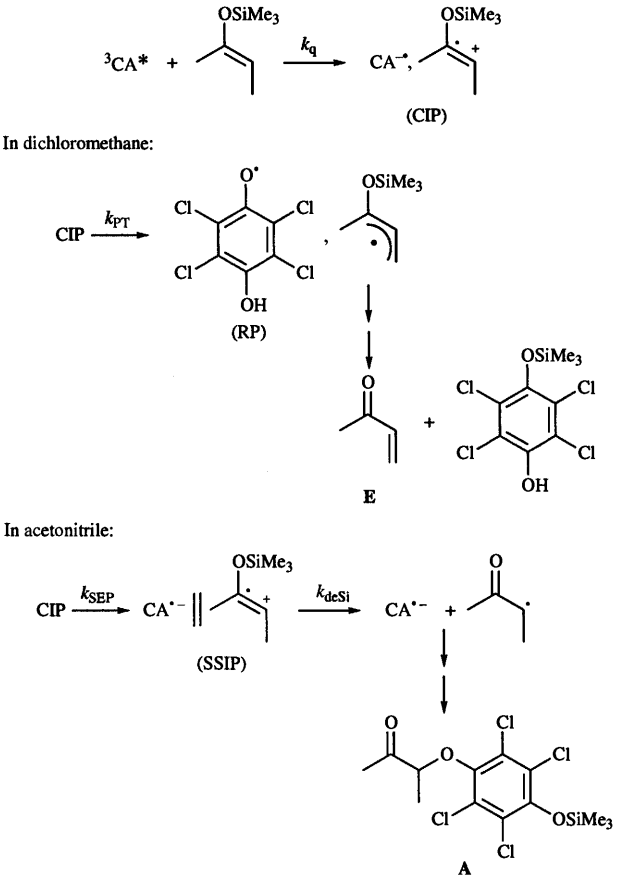

Scheme 6

summarized above in Scheme 6. In dichloromethane, the predominant process is proton transfer (k_{PT}) within the contact radical–ion pair to generate the (silyloxy) cyclohexenyl radical and hydrochloranil radical [eqn. (6)]. The homolytic combination of this radical pair (RP) leads to the α-enone (**E**), together with the monotrimethylsilyl ether of tetrachlorohydroquinone, as described in Scheme 3. In acetonitrile, solvent separation (k_{SEP}) of the contact ion-pair competes effectively with proton transfer (Scheme 2). The resulting (longer-lived) solvent-separated ion pair (SSIP) allows desilylation of the enol silyl ether cation radical (k_{deSi}) to generate the α-ketoalkyl radical and the solvated silyl cation (TMS^+) in Scheme 4. Coupling of this radical with the chloranil anion radical and subsequent silylation by TMS^+ then represents the principal pathway to the oxidative adduct (**A**). The two ion-pair pathways involving proton transfer and solvent separation can thus be modulated by solvent polarity [eqn. (7)] and added salt [eqn. (8)] to direct the course of the reaction to favour either α-enone or adduct.

Experimental

The time-resolved spectroscopic studies were carried out at 23 °C in either dichloromethane or acetonitrile solutions containing the various enol silyl ethers and chloranil at the concentrations employed in the preparative photochemical experiments.[1]

The nanosecond and microsecond time-resolved spectral studies were measured with a Q-switched Nd:YAG laser (Quantel YG 580–10), and a kinetic spectrometer consisting of a 150 W xenon arc lamp, an Oriel 77250 150mm monochromator and a detector consisting of a photomultiplier (Hamamatsu R928) interfaced to a Tektronix 7104 oscilloscope and a Tektronix C1001 digitizing camera. Data acquisition was controlled by a sequence generator, laser controller and backoff unit from Kinetic Instruments. The data were stored and

analysed with the aid of ASYST programs running on a Gateway 2000 personal computer.

The laser source for the picosecond time-resolved transient spectral measurements was a mode-locked Nd:YAG laser (Quantel YG 501-C). Excitation was carried out using the second or third harmonic (532 or 355 nm). The excitation beam traversed a variable delay stage (up to 4.5 ns) before being directed onto the sample cuvette. The analysing light was provided by a continuum beam generated by directing the residual fundamental light (1064 nm) into a 10 cm cuvette containing a 50:50 mixture of H_2O and D_2O. The collimated white light was split into two directions by means of a neutral density filter as a semi-transparent mirror. One beam was directed into the sample cuvette overlapping with the excitation beam to prove the excited sample, while the other served as reference. The sample and reference beams were collected by fibre optic cables and led to a monochromator (Instruments SA HR-320). The signal was recorded on a dual diode array (Princeton Instruments DD-512) that was calibrated with the 436 and 546 nm lines from a mercury lamp. Thus, with each single laser pulse, two spectra (excited sample and reference) were recorded simultaneously and a transient absorption spectrum of the excited species could be computed based on the Beer–Lambert law: $A(\lambda) = \log [I_0(\lambda)/I(\lambda)]$, where $A(\lambda)$ was the transient absorbance at the wavelength λ, and $I_0(\lambda)$ and $I(\lambda)$ were the intensities at the wavelength λ of the reference light and the sample light, respectively. In a typical experiment, 100 spectra were averaged and passed to a personal computer, *via* a Princeton Instruments interface, for data storage, display and analysis.

Acknowledgements

We thank Dr S. Fukuzumi (Osaka) for the results of the *ab initio* calculations. We thank the National Science Foundation, the Texas Advanced Research Program, and the Robert A. Welch Foundation for financial support.

References

1 Part 1: T. M. Bockman, D. Shukla and J. K. Kochi, *J. Chem. Soc., Perkin Trans. 2*, preceding paper.

2 (*a*) E. F. Hilinski and P. M. Rentzepis, *Acc. Chem. Res.*, 1983, **16**, 224; (*b*) N. Mataga, *Pure Appl. Chem.*, 1984, **56**, 1255; (*c*) J. D. Simon, *Rev. Sci. Instrum.*, 1989, **60**, 3597.

3 Compare (*a*) J. D. Simon and K. S. Peters, *J. Am. Chem. Soc.*, 1981, **103**, 6403; (*b*) Y. Hirata, Y. Kanda and N. Mataga, *J. Phys. Chem.*, 1983, **87**, 1659.

4 For the formation of enone (**E**) and adduct (**A**) in dichloromethane and acetonitrile, see Tables 1 and 2 in Ref. 1.

5 Corresponding to the full width at half maximum (fwhm) of the Gaussian bandshape.

6 E. Guerry-Butty, E. Haselbach, C. Pasquier, P. Suppan and D. Phillips, *Helv. Chim. Acta*, 1985, **68**, 912.

7 H. Kobashi, H. Gyoda and T. Morita, *Bull. Chem. Soc. Jpn.*, 1977, **50**, 1731.

8 H. Kobashi, M. Funabashi, T. Kondo, T. Morita, T. Okada and N. Mataga, *Bull. Chem. Soc. Jpn.*, 1984, **57**, 3557.

9 For the absorption spectrum of chloranil anion radical, see R. Gschwind and E. Haselbach, *Helv. Chim. Acta*, 1979, **62**, 941. See also K. Kawai, Y. Shirota, H. Tsubomura and H. Mikawa, *Bull. Chem. Soc. Jpn.*, 1972, **45**, 77; E. F. Hilinski, S. V. Milton and P. M. Rentzepis, *J. Am. Chem. Soc.*, 1983, **105**, 5193; P. P. Levin, P. F. Pluznikov and V. A. Kuzmin, *Chem. Phys. Lett.*, 1988, **147**, 283. See also Ref. 8.

10 J. J. Andre and G. Weill, *Mol. Phys.*, 1968, **15**, 97.

11 (*a*) Note that the white light continuum for the picosecond laser-flash system only extended to 400 nm. (*b*) On the other hand, the extended spectral range of the nanosecond time-resolved spectrometer allowed the reactive intermediates to be observed in the wavelength region from 300 to 900 nm.

12 (*a*) The red-shift in the absorption spectrum of $\mathbf{9}^{\bullet+}$ (which absorbs visible light) is due to the π conjugation of the alkene cation-radical moiety with the phenyl substituent. See R. Rathore and J. K. Kochi, *J. Org. Chem.*, 1996, **61**, 627. (*b*) Indeed, the UV–VIS spectrum of $\mathbf{9}^{\bullet+}$ closely resembles those of styrene cation radicals, as described by L. J. Johnston and N. P. Schepp, *J. Am. Chem. Soc.*, 1993, **115**, 6564.

13 The clear spectral delineation of $\mathbf{9}^{\bullet+}$ in Fig. 1B was obscured by the rapid annihilation of the radical-ion pair in dichloromethane. For a better resolved spectrum of $\mathbf{9}^{\bullet+}$, see Figs. 3B and 6 that were generated in acetonitrile, in which $\mathbf{9}^{\bullet+}$ was substantially longer lived. The subsquent (slower) decay of $CA^{\bullet+}$ and $\mathbf{9}^{\bullet+}$ occurred simultaneously in dichloromethane on the 1 to 3 ns timescale to a weak residual absorption of the hydrochloranil radical (*vide infra*).

14 S. K. Wong, L. Fabes, W. J. Green and J. K. S. Wan, *J. Chem. Soc., Faraday Trans. 1*, 1972, **68**, 2211.

15 Compare T. M. Bockman, K. Y. Lee and J. K. Kochi, *J. Chem. Soc., Perkin Trans. 2*, 1992, 1581.

16 (*a*) In dichloromethane, the half-life for the diffusive separation of the radical–ion pair is $\tau \approx 10^{-8}$ s (*vide infra*). (*b*) The rate constant for a diffusive encounter is 1.5×10^{10} dm^3 mol^{-1} s^{-1}. See S. L. Murov, I. Carmichael and G. L. Hug, *Handbook of Photochemistry*, Dekker, New York, 1993, 2nd ed., p. 207.

17 The relative absorbances at $\lambda_{max} = 450$ and ~ 550 nm in Fig. 3B are in rough accord with the values of $\varepsilon_{max} = 9600$ and 5000 dm^3 mol^{-1} cm^{-1} for $CA^{\bullet-}$ and $\mathbf{9}^{\bullet+}$, respectively, that were formed in more or less equimolar amounts according to eqn. (2). Moreover, the simultaneous growth of the 450 and 550 nm absorbances were roughly comparable ($\tau \sim 0.7$ ns).

18 The quenching studies were carried out in dichloromethane containing 0.0025 M chloranil and 0.001 to 0.01 M enol silyl ether. Under these conditions, the concentration of $^3CA^*$ immediately following the 10 ns laser pulse was $\sim 10^{-6}$ M.

19 Note the quenching rate constant for 2-phenycyclohexanone enol silyl ether **9** in Table 2 (entry 6) was unusually slow (*vide infra*).

20 The decay of $^3CA^*$ ($\lambda_{max} = 510$ nm) in Fig. 4 was comparable to the growth of $HCA^{\bullet}$ ($\lambda_{max} = 430$ nm), since k_q [ESE] was at least two orders of magnitude smaller than k_1 in eqn. (3). (See ref. 18).

21 G. Jones II and W. A. Haney, *J. Phys. Chem.*, 1986, **90**, 5410.

22 The alternative assignment of this transient to the trimethylsilyl-substituted hydrochloranil radical was ruled out by its independent generation. For example, chloranil was photolysed in the presence of 0.05 M hexamethyldisilane in dichloromethane solvent. A transient was observed with two maxima (435 and 340 nm). The UV band of this transient was clearly different from the UV band of authentic $HCA^{\bullet}$, and it was assigned to the silyl-substituted hydrochloranil radical.

23 Compare (*a*) M. Igarishi, T. Ueda, M. Wakasa and Y. Sakaguchi, *J. Organomet. Chem.*, 1991, **421**, 9; (*b*) M. T. Craw, A. Alberti, C. M. Depew and J. K. S. Wan, *Bull. Chem. Soc. Jpn.*, 1985, **58**, 3675.

24 (*a*) I. Carmichael and G. L. Hug, *J. Phys. Chem. Ref. Data*, 1986, **15**, 1; (*b*) R. Bonneau, I. Carmichael and G. L. Hug, *Pure Appl. Chem.*, 1991, **63**, 289.

25 J. K. Hurley, N. Sinai and H. Linshitz, *Photochem. Photobiol.*, 1983, **38**, 9.

26 The pair of bands at $\lambda_{max} = 540$ and 370 nm were thus assigned to $\mathbf{9}^{\bullet+}$ on the basis of (*a*) their concurrent rise with $CA^{\bullet-}$ to suggest that they were formed by the same electron-transfer process, (*b*) their simultaneous decay with the same first-order rate constant and (*c*) their similarity to a variety of related styrene cation radicals.[12b] (*d*) Furthermore, the same two bands were observed upon the photoinduced electron transfer of enol silyl ether **9** (in the presence of benzophenone and 1,2,4,5-tetracyanobenzene) by the procedure described by P. K. Das, *J. Chem. Soc., Faraday Trans. 1*, 1983, **79**, 1135.

27 (*a*) V. O. Brede, W. Helmstreit and R. Mehnert, *J. Prakt. Chem.*, 1974, **316**, 402; (*b*) C. Chatgilialoglu, in *Handbook of Photochemistry*, ed. J. C. Scaiano, CRC Press, Boca Raton, FL, 1989, vol II, p 1.

28 (*a*) It is important to note that spectral decay of $\mathbf{9}^{\bullet+}$ according to eqn. (4) occurred with essentially the same first-order rate constant as that of $\mathbf{9}^{\bullet+}$ generated independently [see ref. 26 (*d*) with $k_{ESE} = 1.8 \times 10^7$ s^{-1}], (*b*) An alternative explanation for the decay of $\mathbf{9}^{\bullet+}$ in Fig. 6 involves its facile reaction with (neutral) **9**. Although an analogous coupling reaction has been observed for various styrene cation radicals,[12b] it is unlikely in this case, in view of (i) the unreactivity of β-disubstitued styrene cation radicals such as $\mathbf{9}^{\bullet+}$ towards dimerization[12b] and (ii) the absence of dimers of **9** among the reaction products.[1]

29 (*a*) On the timescale of 10–200 ns, the spectrum of $CA^{\bullet-}$ appeared as a minor tail on the red edge (460–480 nm) of the spectral band of hydrochloranil radical (compare Figs. 4 and 5). (*b*) However, the presence of $CA^{\bullet-}$ was readily monitored at 480 nm, since its extinction coefficient ($\varepsilon_{480} = 3600$ dm^3 mol^{-1} cm^{-1}) was substantially larger than that ($\varepsilon_{480} \approx 500$ dm^3 mol^{-1} cm^{-1}) of the hydrochloranil radical.

30 For the concomitant formation of the enol silyl ether cation radical $ESE^{\bullet+}$, see Figs. 1B, 3B and 6.

31 (*a*) Electron transfer to triplet chloranil has been identified for donors such as naphthalene[9a] and other arenes,[8,32] alkenes[33] and alkylmetals.[34] In some of these cases, the intermediacy of a triplet exciplex has been established. In the absence of definitive spectral or luminescence studies, a distinction between a radical–ion pair and a polar exciplex is very hard to draw.[35] The anion radical of chloranil within the radical–ion pair, as observed on the picosecond and nanosecond timescales, appears identical to that formed independently, and there is no characteristic long-wavelength band as found for chloranil exciplexes with alkylbenzene donors.[32] On the other hand, the influence of electronic coupling between the radical ions in the photogenerated ion pair in directing the various charge-annihilation reactions should not be minimized. (*b*) Although the radical–ion pair in eqn. (5) is formed in its triplet state, all subsequent reactions that generate radical pairs are unaffected by any (such) spin multiplicity. However, for its restriction on back electron transfer to the singlet ground state [eqn. (9)], see ref. 47 in Part I.[1]

32 T. Tahara and H. Hamaguchi, *J. Phys. Chem.*, 1992, **96**, 8252.

33 H. Kobashi, H. Gyoda and T. Morita, *Bull. Chem. Soc. Jpn.*, 1977, **50**, 1731.

34 S. Kozima, H. Fujita, T. Hitomi, K. Kobayashi, K. Kobayashi and M. Kawanisi, *Bull. Chem. Soc. Jpn.*, 1980, **53**, 2953.

35 R. A. Caldwell and D. Creed, *Acc. Chem. Res.*, 1980, **13**, 45.

36 Accordingly, the quantum yield for the formation of chloranil anion radical in Table 1 relates directly to the efficiency of radical–ion pair formation in eqn. (5), and it is therefore referred to hereafter as Φ_{RIP}.

37 Calculated using the relationship:[38] $E_{red}°(^3CA*) = E_{red}°(CA) + E_T/F$, where $E_{red}°$ is the reduction potential of ground-state chloranil (0.02 in CH_3CN)[39] and E_T is the energy of the triplet excited state (206 kJ mol^{-1}).[40]

38 D. Rehm and A. Weller, *Ber. Bunsenges. Phys. Chem.*, 1969, **73**, 834.

39 C. K. Mann and K. K. Barnes, *Electrochemical Reactions in Nonaqueous Systems*, Dekker, New York, 1970.

40 See Murov *et al.* in, Ref 16*b* p. 19.

41 Silyl enol ethers have been identified as viable electron donors by the combination of spectral, electrochemical and photoionization methods. See R. Rathore and J. K. Kochi, *Tetrahedron Lett.*, 1994, **35**, 8577.

42 (*a*) F. D. Lewis and J. R. Petisce, *Tetrahedron*, 1986, **42**, 6207; (*b*) F. D. Lewis, *Acc. Chem. Res.*, 1986, **19**, 401.

43 A. Albini, E. Fasani and N. Alessandro, *Coord. Chem. Revs.*, 1993, **125**, 269.

44 D. R. Arnold, P. C. Wong, A. J. Maroulis and T. S. Cameron, *Pure Appl. Chem.*, 1980, **52**, 2609.

45 G. Jones II, W. A. Haney and X. T. Phan, *J. Am. Chem. Soc.*, 1988, **110**, 1922.

46 R. Mehnert, O. Brede and G. Cserep, *Radiat. Phys. Chem.*, 1985, **26**, 353.

47 (*a*) Electron transfer quenching of $^3CA*$, combined with the proton transfer in eqn. (6), constitutes a two-step (EC) sequence for hydrogen atom transfer from silyl ether to chloranil triplet. Hydrogen atom transfers are ubiquitous in both the thermal[48] and photochemical[49] reactions of quinones. (*b*) In contrast to the clearcut two-step sequence observed upon quenching of $^3CA*$ with ESE, there is usually an ambiguity as to whether H-atom transfer occurs in one or two distinct steps.

48 Compare (*a*) S. Perrier, S. Sankararaman and J. K. Kochi, *J. Chem. Soc. Perkin Trans.* 2, 1993, 825; (*b*) H. D. Becker, in *The Chemistry of the Quinonoid Compounds*, Part 1, ed. S. Patai, Wiley, New York, 1974, p. 335.

49 K. Maruyama and A. Osuka, in *The Chemistry of Quinonoid Compounds*, eds. S. Patai and Z. Rappoport, Wiley, New York, 1988, Part 2, p. 759.

50 (*a*) T. W. Bentley and P. Von R. Schleyer, *Adv. Phys. Org. Chem.*, 1977, **14**, 1; (*b*) J. E. Gordon, *The Organic Chemistry of Electrolyte Solutions*, Wiley, New York, 1975, p. 341f; (*c*) M. Szwarc, in *Ions and Ion Pairs in Organic Reactions*, ed. M. Szwarc, Wiley, New York, 1972, p. 15f.

51 J. Mattay and M. Vondenhof, *Top. Curr. Chem.*, 1991, **159**, 219.

52 (*a*) R. A. McClelland, V. M. Kanagasabapathy, N. S. Banait and S. Steenken, *J. Am. Chem. Soc.*, 1991, **113**, 1009; (*b*) F. L. Cozens, N. Mathivanan, R. A. McClelland and S. Steenken, *J. Chem. Soc., Perkin Trans.2*, 1992, 2083; (*c*) L. E. Manring and K. S. Peters, *J. Phys. Chem.*, 1984, **88**, 3516; (*d*) K. G. Spears, T. H. Gray and D. Haung, *J. Phys. Chem.*, 1986, **90**, 779; (*e*) E. Haselbach, E. Vauthey and P. Suppan, *Tetrahedron*, 1988, **44**, 7335.

53 K. S. Peters and J. D. Simon, *J. Am. Chem. Soc.*, 1983, **105**, 4879.

54 J. M. Masnovi and J. K. Kochi, *J. Am. Chem. Soc.*, 1985, **107**, 7880.

55 C. Devadoss and R. W. Fessenden, *J. Phys. Chem.*, 1990, **94**, 4540.

56 T. Yabe and J. K. Kochi, *J. Am. Chem. Soc.*, 1992, **114**, 4491.

57 S. Winstein, P. E. Klinedinst, Jr. and G. C. Robinson, *J. Am. Chem. Soc.*, 1961, **83**, 885.

58 S. Winstein and E. Clippinger, *J. Am. Chem Soc*, 1956, **78**, 2784.

59 (*a*) A. H. Fainberg and S. Winstein, *J. Am. Chem. Soc.*, 1956, **78**, 2780; (*b*) A. H. Fainberg, G. C. Robinson and S. Winstein, *J. Am. Chem. Soc.*, 1956, **78**, 2777; (*c*) S. Winstein and A. H. Fainberg, *J. Am. Chem. Soc.*, 1958, **80**, 459.

60 A. D. Allen, M. Fujio, O. S. Tee, T. T. Tidwell, Y. Tsuji, U. Tsuno and K. Yatsugi, *J. Am. Chem. Soc.*, 1995, **117**, 8974.

61 The quantum yield for *free ions* is given by the quantum yield of $CA^{\bullet -}$ at zero salt concentration (in Fig. 8), and is very small (< 0.01).

62 E. Haselbach, P. Jacques, D. Pilloud, P. Suppan and E. Vauthey, *J. Phys. Chem.*, 1991, **95**, 7115.

63 The complete separation of $CA^{\bullet -}$ and $2^{\bullet +}$ in acetonitrile precludes a salt-effect study, and it is not possible to identify definitively the initially-formed ion pair in this solvent. It is likely that the contact radical–ion pair is first formed in both solvents, in view of the identity of the quenching processes in dichloromethane and acetonitrile.

64 See Table 4 in Ref. 1.

65 This exchange occurs at high (*ca.* 0.1 M) salt concentrations (normal salt effect) and should be distinguished from the interception of solvent-separated ion pairs (special salt effect) discussed earlier.

66 The process by which the radical pair in Scheme 3 yields the enone is not clear. One attractive possibility is electron transfer from the trimethylsiloxycyclohexenyl radical to HCA$^{\bullet}$. The resulting ion-pair ($ETMS^+$, HCA^-) would yield the observed products upon transfer of TMS^+ from the cation to the anion.

67 P. G. Gassman and K. J. Botorff, *J. Org. Chem.*, 1988, **53**, 1097.

68 (*a*) A. Albini, M. Mella and M. Freccero, *Tetrahedron*, 1994, **50**, 575; (*b*) E. Fasuni, D. Peverali and A. Albini, *Tetrahedron Lett.*, 1994, **49**, 9275.

69 (*a*) This desilylation is presumably assisted by nucleophilic attack of the solvent on the cation radical. Acetonitrile is a nucleophilic solvent according to the Gutmann scale of solvent donicity (see U. Mayer and V. Gutmann, *Struct. Bonding*, 1992, **12**, 113). Note that the desilylation of enol silyl ether cation radicals is approximately 10^4 times faster in acetonitrile than in non-nucleophilic solvents such as dichloromethane. See M. Schmittel, M. Keller and A. Burghart, *J. Chem. Soc, Perkin Trans. 2*, **1995**, 2327; (*b*) E. Baciocchi, T. Del Giacco, F. Elisei and M. Ioele, *J. Org. Chem.*, 1995, **60**, 7974.

70 (*a*) Y. Hirata, Y. Kanda and N. Mataga, *J. Phys. Chem.*, 1989, **93**, 6575; (*b*) T. Asahi, and N. Mataga, *J. Phys. Chem.*, 1989, **93**, 6575; (*c*) T. Asahi, N. Mataga, Y. Takahashi and T. Miyashi, *Chem. Phys. Lett.*, 1990, **171**, 309; (*d*) H. Miyasaka, K. Morita, K. Kamada and N. Mataga, *Bull. Chem. Soc. Jpn.*, 1990, **63**, 3385; (*e*) T. Asahi and N. Mataga, *J. Phys. Chem.*, 1991, **95**, 1956.

71 (*a*) I. R. Gould, L. J. Mueller and S. Farid, *Z. Phys. Chem.*, 1991, **170**, 143; (*b*) I. R. Gould, R. W. Young, L. J. Mueller and S. Farid, *J. Am. Chem. Soc.*, 1994, **116**, 8176, (*c*) I. R. Gould, R. H. Young, L. J. Mueller, A. C. Albrecht and S. Farid, *J. Am. Chem. Soc.*, 1994, **116**, 8188; (*d*) A. B. Myers, *Chem. Phys.*, 1994, **180**, 215.

72 (*a*) M. R. Wasielewski, in *Photoinduced Electron Transfer*, eds. M. A. Fox and M. Chanon, Elsevier, New York, 1988 p. 161; (*b*) K. I. Zamaraev and R. F. Khairutdinov, *Top. Curr. Chem.*, 1992, **163**, 4; (*c*) E. F. Hilinski, J. M. Masnovi, C. Amatore, J. K. Kochi and P. M. Rentzepis, *J. Am. Chem. Soc.*, 1983, **105**, 6167.

73 The separation rate constant for the ion-pair comprised anthracene cation and trinitromethide anion, *i.e.* [A^+, T^-] in dichloromethane ($8–9 \times 10^8$ s^{-1})[56] is considerably faster than k_{SEP} for [$CA^{\bullet -}$, $2^{\bullet +}$]. The radical–ion pair may be bound together more strongly than the non-radical [A^+, T^-] pairs. The rates of association of ($2–5 \times 10^7$ s^{-1}) for the solvent-separated [A^+, T^-] pairs are comparable to that of the [$CA^{\bullet -}$, $2^{\bullet +}$] solvent-separated ion pair.

74 Ketene silyl acetals, [$(R_3SiO)_2C{=}CR'_2$], are oxidized to cation radicals which are completely distonic. These species have 90° dihedral angles around the 'double bonds'. See S. Fukuzumi, M. Fujita, J. Otera and Y. Fujita, *J. Am. Chem. Soc.*, 1992, **114**, 10241.

75 M. R. Novice, H. R. Seikaly, A. D. Seiz and T. T. Tidwell, *J. Am. Chem. Soc.*, 1980, **102**, 5835.

76 This 'inverted' trend as opposed to the 'normal' increase in rate with increasing driving force is predicted by the Marcus theory of electron transfer.[77]

77 R. A. Marcus, *J. Chem. Phys.*, 1965, **43**, 679. See also P. Suppan, *Top. Curr. Chem.*, 1992, **163**, 95.

78 P. R. Rich and D. S. Bendall, *Biochim. Biophys. Acta*, 1980, **592**, 506.

Paper 6/00834H
Received 5*th February* 1996
Accepted 29*th March* 1996